Major research project:

Characterizing the role of nuclear pyruvate dehydrogenase upon mutant HRAS expression

Student:	Esmée Krap
Student ID:	7078080
Supervisor:	Dr. Enric Mocholi, Coffer lab UMCU
Study program:	MSc Science and Business Management, Utrecht University
Date:	21st June, 2024

Characterizing the role of nuclear pyruvate dehydrogenase upon mutant HRAS expression

GRAPHICAL ABSTRACT

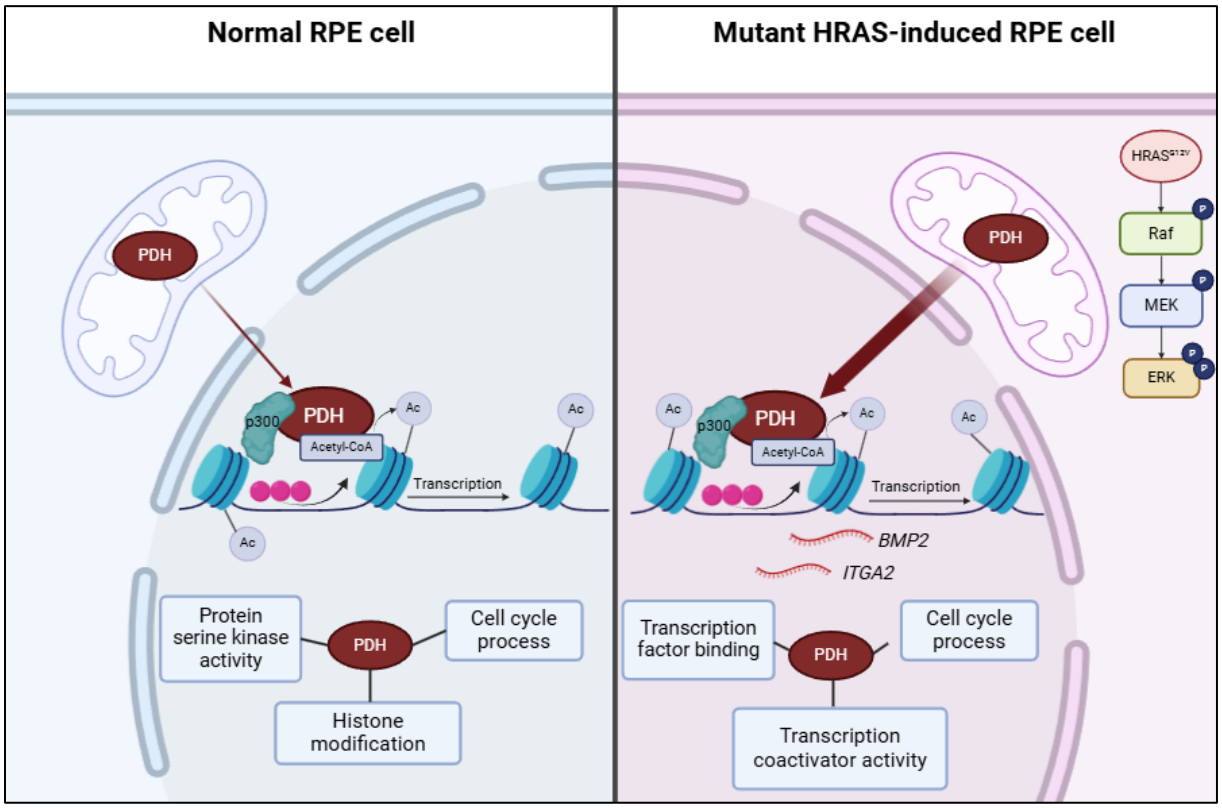

ABSTRACT

Oncogenic transformation can be caused by mutations in the *Ras* gene, present in 30% of all human cancers. Mutations in Harvey RAS (HRAS), an isoform of *Ras*, induce changes in metabolism, epigenome remodeling, and the transcriptome, enabling cells to grow and proliferate continuously. Cancer cells upregulate aerobic glycolysis to generate biosynthetic precursors necessary for rapid proliferation, called the Warburg effect. Additionally, glycolysis is important for histone acetylation, inducing an open chromatin structure. Earlier research showed that the mitochondrial enzyme pyruvate dehydrogenase (PDH) can produce acetyl-CoA in the nucleus, facilitating histone acetylation. This study investigates how PDH plays a role in the nucleus upon mutant HRAS expression. The findings demonstrate that when RPE cells express mutant $HRAS^{G12V}$, there is translocation of PDH to the nucleus. In the nucleus of mutant HRAS-induced cells, the interactome of PDH is reconfigured. The nuclear interactome of PDH includes enriched proteins involved in transcriptional regulation after mutant HRAS induction. Furthermore, PDH is located near the promotor regions of actively transcribed genes expressed after mutant HRAS transformation. Together, this might indicate that PDH could play a role in epigenome remodeling and gene

transcription during mutant HRAS expression. Interference with nuclear PDH might offer therapeutic targets for cancer proliferation.

LAYMAN'S SUMMARY

The formation of a normal cell into a cancer can be initiated by mutations in genes that regulate essential cell processes. When the HRAS gene is mutated, it changes the genes expressed in the cell to make it grow uncontrollably. Mutated HRAS also impacts the metabolism of the cell, increasing glycolysis. Cancer cells use glycolysis to produce nutrients they need to grow rapidly, called the Warburg effect. Pyruvate dehydrogenase (PDH) is a glycolytic enzyme that produces a metabolite called acetyl-CoA. Acetyl-CoA is important for the expression of genes. How PDH plays a role in the nucleus of cancer cells is not understood. The results show that PDH is transported to the nucleus when a cell becomes cancerous. In the nucleus, the proteins that surround PDH change when mutant HRAS is activated, including more proteins involved in gene expression. Additionally, PDH is located close to the start site of genes known to be expressed by the cancer cell. This indicates that PDH might be important for these genes to be turned 'on'. Understanding how PDH changes in cancer cells, can help in developing ways to try to slow down or even halt cancer growth.

INTRODUCTION

Metabolic and epigenetic reprogramming are hallmarks of cancer, which allow tumor cells to grow and proliferate continuously (Hanahan & Weinberg, 2011). Mutations in the *Ras* gene can cause different types tumor development (Der et al., 1982; Parada et al., 1982). Activation mutations in a *Ras* gene are present in 30% of all human tumors (Alberts et al., 2018). Harvey *Ras* (HRAS) is a member of the *Ras* family and functions as a molecular switch in pathways that regulate cell proliferation and survival. Mutations in HRAS can cause hyperactivation of the MAPK signaling pathway (Pylayeva-Gupta et al., 2011). This causes downstream proteins to be permanently phosphorylated, which induces changes in epigenome remodeling and the transcriptome. This results in increased cell proliferation and growth (Prior et al., 2012; Segeren et al., 2022). The disruption of the epigenome plays a key role in maintaining tumor proliferation and growth (Shen & Laird, 2013). Previous research has shown that the induction of mutant $HRAS^{G12V}$ induces changes in the transcriptome (Segeren et al., 2022). By investigating how epigenome remodeling and the change transcription during oncogenic transformation is regulated, new therapeutic could be developed to inhibit oncogenic transformation.

The activation of oncogenes often leads to metabolic alterations (Kroemer & Pouyssegur, 2008; Hanahan & Weinberg, 2011). It was first described by Warburg in 1927 that even in the presence of oxygen tumor cells heavily rely on glycolysis, referred to as aerobic glycolysis (Warburg et al., 1927).

Mutated HRAS induces alterations in metabolism, including increased glycolytic activation (Myllymäki et al., 2024). Although it was shown that glucose metabolism is not the biggest contributor to cell mass, glycolysis is essential for other metabolic functions, providing ATP and intermediates for biosynthetic processes (Hosios et al., 2016). Moreover, previous research has reported that glycolysis might be important for the reprogramming of the epigenome. It was found that glycolysis is important for maintaining histone acetylation and an open chromatin structure (Liu et al., 2015; Moussaieff et al., 2015). The positive charge of histone proteins is reduced by histone acetylation, which reduces the attraction to negatively charged DNA, causing the chromatin to open. The open state of the chromatin, euchromatin, allows for the binding of transcription factors to the DNA, causing changes in gene expression (Lee et al., 1993; Ralston & Brown, 2008). Histone acetylation is often deregulated in cancer (Falkenberg & Johnstone, 2014). An important player during histone acetylation is acetyl-CoA, which is a donor of acetyl groups needed for acetylation. Thus, acetyl-CoA is an important metabolite for the maintenance of histone acetylation. Acetyl-CoA contains high-energy thioester bonds, making it very unstable and impermeable to membranes. Therefore, acetyl-CoA is produced in the compartment where it is used (Sutendra et al., 2014). The compartmentalization of metabolism is beneficial to create an environment that contains the required conditions, as well as protection and the controlled regulation of metabolic pathways (Bar-Pelled et al., 2022). Nuclear compartmentalization of metabolite production in the nucleus is important for the regulation of gene expression (Bar-Pelled et al., 2022). There are nuclear pools of substrates, including acetyl-CoA, important for histone modification by histone acetyltransferases (Campbell & Wellen, 2018). Metabolite levels can provide feedback for transcriptional regulators (Bar-Pelled et al., 2022). The spatial separation of pathways regulates gene expression efficiently in response to metabolic changes, thereby connecting metabolism with the mechanisms that control transcription (Bar-Pelled et al., 2022).

Furthermore, acetyl-CoA is mainly produced in the mitochondria by pyruvate dehydrogenase (PDH), in a process called pyruvate decarboxylation. PDH is a large enzyme complex that consists of subunits PDC-E1, E2 and E3 (Milne, 2013). PDH uses pyruvate produced by glycolysis as a substrate for acetyl-CoA production. Acyl-CoA synthetase short-chain family member 1 (ACSS1) is another mitochondrial enzyme that can ligate acetate to CoA (Schlug et al., 2016). In the cytoplasm and nucleus, acetyl-CoA can be produced by acyl-CoA synthetase short-chain family member 2 (ACSS2) (Schlug et al., 2016). ATP-citrate lyase (ACLY) is an enzyme present in the cytosol and nucleus that can convert citrate to acetyl-CoA (Sivanand et al., 2017). It was shown that both ACLY and ACSS2 can be localized to the nucleus and produce acetyl-CoA to facilitate the acetylation of histones and facilitating gene transcription (Wellen et al., 2009; Bulusu et al., 2017; Li et al., 2017). Additionally, research has

shown that isolated liver cancer cell nuclei contained glycolytic enzymes and were able to convert glucose into pyruvate (Sun et al., 2019). Besides ACLY and ACSS2, both present in the cytoplasm and nucleus, it was reported that PDH can translocate to the nucleus as well when cells are induced with mitochondrial stress (Sutendra et al., 2014). Moreover, the translocation of PDH to the nucleus is important for the regulation of histone acetylation (Li et al., 2022; Sivanand et al., 2018; Sutendra et al., 2014). It was shown that the translocation of PDH to the nucleus was increased during embryonic development and in activated T cells, where it was reported to be important for the acetylation of histones (Mocholi et al., 2023; Zhou et al., 2020). The inhibition of glycolysis in activated T cells caused a decrease in H3K27 acetylation and epigenome remodeling (Mocholi et al., 2023). Recently a paper has shown that nuclear PDH can associate with mediator complexes facilitating transcription, suggesting that PDH is important for local production of acetyl-CoA (Russo et al., 2024). It was suggested that the translocation of PDH to the nucleus might play a role in situations where cellular metabolism and proliferation are altered, such as cancer (Sutendra et al., 2014).

Metabolic alterations can regulate chromatin modifications and gene expression levels (Liu et al., 2015). However, the regulation of these processes by acetyl-CoA-producing enzymes in cancer cells are not very well known. Therefore, investigating the role of nuclear acetyl-CoA-producing enzymes in the nucleus is important to have a clearer idea about how acetyl-CoA is produced and utilized for histone acetylation during mutant HRAS transformation. The goal of this report is to characterize the role of nuclear acetyl-CoA-producing enzymes upon mutant HRAS expression. To assess the role of acetyl-CoA-producing enzymes in the nucleus of cancer cells, Retinal Pigment Epithelial (RPE) that bear an inducible construct containing oncogenic $HRAS^{G12V}$ are utilized in this study. $HRAS^{G12V}$-induced RPE cells proliferate and progress faster through the cell cycle than normal cells, inducing tumor formation in mice (Segeren et al., 2022). Therefore, it can be used as a model to investigate oncogene-driven tumor transformation. In this study, the nuclear levels of acetyl-CoA-producing enzymes after mutant HRAS expression in RPE cells were studied. The findings demonstrate that PDC-E1, a subunit of PDH, is translocated to the nucleus in $HRAS^{G12V}$-induced cells. Subsequently, the nuclear interactome of PDC-E1 and the associated chromatin locations were investigated using a PDH-BioID construct that enables close-proximity labeling. Proteomics analysis revealed that $HRAS^{G12V}$ expression induces reconfiguration of the nuclear interactome of PDC-E1 in RPE cells. The nuclear interactome of PDH included enriched proteins involved in transcriptional regulation after mutant HRAS expression. Lastly, the PDH-BioID construct was used to identify the associated chromatin location. RT-qPCR data of ChIP samples demonstrate that PDH is located near the promotor regions of actively transcribed genes *BMP2* and *ITGA2* in mutant HRAS-induced RPE cells.

Using these metabolic alterations in cancer cells may offer therapeutic targets to inhibit oncogenic transformation.

MATERIALS AND METHODS

Cell culture

The human non-transformed RPE-1 cells with inducible oncogenic HRAS ($HRAS^{G12V}$) under the control of a Tet repressor were kindly provided by Kate Wierenga-Royer from the lab of Bart Westendorp, Utrecht University (UU). The RPE-1 $HRAS^{G12V}$ cell lines containing the PDH-BioID or LaminB-BioID were both generated through lentiviral transduction. All cell lines were cultured in Dulbecco's Modified Eagle's Medium (DMDM) media, supplemented with 10% Fetal Bovine Serum (FBS) and 1% penicillin/streptomycin. To induce $HRAS^{G12V}$ expression, 1 µM of doxycycline (Sigma, D9891-1G) was administered to the cells. 6,8-bis(benzylthio)octanoic acid (Sigma-Aldrich, SML0404), an inhibitor of PDH, was used at a concentration of 150 µM for 24h. Dichloroacetate (DCA) (Tocris Bioscience, 2755), an inhibitor of PDK, was used at a concentration of 5 µM. The cells were cultured at 37 ˚C, 5% CO_2.

Seahorse assay

To perform a seahorse assay, 50.000 RPE cells were plated with or without doxycycline on a 24 seahorse plate in XF media, containing 10 mM glucose, 2 mM L-glutamine, and 1 mM sodium pyruvate. The cells were treated with tamoxifen for 48h. For measurement of the extracellular acidification rates (ECAR) and oxygen consumption rates (OCR), an XF-24 Extracellular Flux Analyzer (Seahorse Bioscience) was used. Under basal conditions, ECAR was measured in response to 30 mM glucose, 1 µM oligomycin (Merck Millipore, 495455), and 50 mM of 2DG (Sigma-Aldrich, D8375-5G). The OCR was measured in response to 1 µM oligomycin, 10 mM FCCP (Abcam, ab120081), and 1 µM Rotenone (Merck Millipore, R8875).

Measurement of acetyl-CoA levels

In ten cm dishes, 1 million RPE cells were plated with or without doxycycline for 48h. The cells were treated with 48h of tamoxifen. The intracellular acetyl-CoA levels in RPE cells with or without doxycycline were measured by using an acetyl-CoA assay kit (Biovision, Milpitas CA, K317-100), following the manufacturer's protocol.

Nuclear and cytoplasmic extraction

To obtain nuclear and cytoplasmic lysates, the Nuclear Extract Kit (Active Motif, 40010) was used according to the manufacturer's protocol, adjusted to RPE cells. RPE cells were plated in three ten cm

dishes with or without doxycycline. After 48h the cells were harvested and washed with phosphate-buffered saline (PBS). To prepare total cellular lysates, radioimmunoprecipitation assay (RIPA) buffer (1% Trition-X 100, 1% sodium deoxycholate, 0,1% SDS, 0.15 M NaCl, 0.01 M sodium phosphate at pH 7.2) was used with 1X HALT protease inhibitor. The cells were centrifuged at 400 rcf for five minutes. 750 µl of 1X Hypotonic buffer was added to the cell pellet and the cells were incubated on ice for 30 minutes. Then 37,5 µl of detergent was added and cell lysis was confirmed under the microscope. The cells were centrifuged at 16.000 rcf for 30 seconds and the cytoplasmic fraction was collected. The nuclear pellet was resuspended in 500 µl 1X Hypotonic buffer and centrifuged at 16.000 rcf for 30 seconds. This washing step was repeated twice. Subsequently, the nuclear pellet was resuspended in 150 µl Complete lysis buffer and disrupted using a Dounce homogenizer. The nuclei were incubated on ice for 30 minutes. To collect the nuclear extract, nuclei were centrifuged at 16.000 rcf. All samples were stored at -20 ˚C until use.

Western blot

Total cellular lysates were prepared using RIPA buffer with 1X HALT protease inhibitor. The quantification of proteins was determined with the Lowry assay (Greenfield et al, 2018). 1X Sample buffer was added to the samples before boiling them for 5 minutes. Samples were loaded on gel containing 12,5% acrylamide and electrophoresed for 90-120 minutes at 90 Volt. To transfer the proteins to a Mini-size LF PVDF membrane, Trans-Blot Turbo Transfer System RTA Transfer Kits (Biorad) was used according to the manufacturer's protocol. The membrane was blocked in TBST-T with 5% ELK. Primary antibodies were diluted 1:1000 in 3% bovine serum albumin (BSA) (Sigma-Aldrich, 000282903) in TBST-T and incubated overnight at 4 ˚C. All antibodies utilized in this study are described in **Supplementary Table S1**. Secondary antibodies were diluted 1:5000 or 1:20000 in TBST-T with 5% ELK for 1 hour at room temperature (RT). After washing, the images were acquired with either the ChemiDoc Touch Imaging System (Biorad) using SuperSignal chemiluminescent HRP substrate Dura (Thermo Scientific, 34076), or the LI-COR Odessey imaging system (Westburg) using fluorophore-coupled antibodies. ImageJ was used to quantify the bands (Abramoff et al., 2004).

Liquid chromatography-mass spectrometry (LC-MS)-based proteomics

RPE cells containing the PDH-BioID or LaminB-BioID were plated in nine ten cm dishes for 48h with or without doxycycline, where the plate was 80-90% confluent when harvesting. 50 µM of D-biotin was added 2h before harvesting. After 48h the cells were harvested and washed with PBS. The nuclear fraction was obtained as described earlier. Streptavidin Agarose Resin beads (Thermo Scientific, 20349) were added to the nuclear fractions and rotated overnight at 4 ˚C. The beads were washed with RIPA buffer containing 1X HALT protease inhibitor. The last wash was done with PBS and the

liquid was aspirated until the beads were dry. The samples were stored at -20 ˚C before they were sent for LC-MS-based proteomics.

Chromatin immunoprecipitation (ChIP)-qPCR

RPE cell lines containing the PDH-BioID or LaminB-BioID were plated in nine ten cm dishes for 48h with or without doxycycline, where the plate was 80-90% confluent when harvesting. 50 µM of D-biotin was added to the plates 2h before harvesting. After 48h the cells were harvested and washed with PBS. The cells were fixated using 2% formaldehyde. To stop the fixation, 2M glycine was added to the cells. After washing with PBS containing 5% BSA, the cells were lysed with nuclear isolation buffer (50 mM TRIS, 150 mM NaCl, 5 mM EDTA, 0,5% NP-40, and 1% TX-100). The isolated nuclei were lysed in sonication buffer (20 mM TRIS 7.5 pH, 150 mM NaCl, 2 mM EDTA, 1% NP40 and 0.3% SDS), and sheared with Covaris (duty cycle 20%, intensity 3, cycles per burst 200, cycle time 60 sec, cycles 8). The supernatant was diluted 1:1 in dilution buffer (20 mM TRIS pH 8, 150 mM NaCl, 2 mM EDTA, Triton-X). Streptavidin Agarose Resin beads (Thermo Scientific, 20349) were added to the chip lysates and rotated overnight at 4 ˚C. The samples were reversed crosslinked using 1% SDS, 100 mM NaHCO3, 200 mM NaCl and 300 µg proteinase K/ml. To purify the DNA the ChIP DNA Clean & Concentrator kit (ZYMO) was used according to the manufacturers protocol. The ChIP DNA was used for RT-qPCR or sequencing. The immunoprecipitated samples were normalized to the input DNA and a Negative region 3 primer. RT-qPCR was used to determine promotor regions in the samples. The primer sequences are listed in **Supplementary Table S2**.

RNA isolation, cDNA synthesis and quantitative PCR

Total RNA was isolated from cells using the RNeasy Mini Kit (QIAGEN, cat. nos. 74104 and 74106) according to the manufacturer's quick-start protocol. The RNA was quantified using the Nanodrop and cDNA was synthesized using iScript reverse transcriptase (Biorad, L007877B) and 5x iScript reaction mix (Biorad, L010174C) according to the manufacturer's datasheet. The cDNA was synthesized using the Biometra T3000 Thermocycler (Labrepco). mRNA expression was quantified using real-time quantitative PCR (qRT-PCR). Real-time PCR was performed with FastStart SYBR Green (Roche), using the Biorad CFX96. Relative RNA quantities were calculated using the ΔΔCT method. Expression of each gene was normalized to housekeeping gene actin. All primers utilized for the qRT-PCR in this report are described in **Supplementary Table S3**.

Statistical analysis

The statistical analysis of the data was done in GraphPad Prism version 9.3.1. Unpaired Student's t-test, or one-way ANOVA with Tukey's multiple comparison tests were used to analyze differences between groups. Ns means not significant, *P<0.05, **P<0.01, and ***P<0.001.

RESULTS

Induction of HRAS^{G12V} in RPE cells induces transcriptional and metabolic changes

To explore the role of nuclear acetyl-CoA-producing enzymes upon mutant HRAS expression, human non-transformed RPE-1 cells with inducible oncogenic HRAS (HRAS^{G12V}) under the control of a Tet repressor were utilized. We evaluated whether this model induces metabolic and transcriptional changes upon HRAS^{G12V} expression in RPE cells. Administration of doxycycline for 48h to RPE cells significantly induced the expression of HRAS in the cells (**Figure 1A**). This caused hyperactivation of the MAPK pathway, shown by increased levels of phosphorylation of downstream target pERK1/2 in mutant HRAS-induced cells (**Figure 1B**). RNA sequencing data showed that the induction of HRAS^{G12V} in RPE cells causes major changes in the transcriptome, including upregulation of bone morphogenetic protein 2 (*BMP2*) and integrin alpha2 (*ITGA2*) (Segeren et al., 2022). *BMP2* is involved in regulating proliferation, differentiation, and survival of cells. Therefore, when *BMP2* is dysregulated, this can lead to cancer development (Davis et al., 2015). *ITGA2* is an integrin, involved in cell communication. When *ITGA2* is differently expressed, this can lead to the uncontrolled proliferation and invasion of the cell (Gregori et al., 2023). To investigate whether the induction of mutant HRAS causes upregulation of relevant genes, the expression of BMP2 and ITGA2 was measured after 48h of doxycycline administration. The results showed that *BMP2* expression was significantly increased, and *ITGA2* expression was slightly increased in RPE cells treated with doxycycline (**Figure 1C, D**).

Alterations in the metabolism are a hallmark of cancer cells (Hanahan & Weinberg, 2011). Cancer cells upregulate glycolysis to facilitate rapid cell growth and division (Warburg et al., 1927). To evaluate the metabolic capacity of RPE cells induced with HRAS^{G12V}, Seahorse analysis was performed. The OCR and ECAR were measured, as indicators for mitochondrial respiration and glycolysis, respectively. The OCR was preserved after doxycycline administration compared to the non-treated cells, which indicates that mitochondrial respiration is not altered upon mutant HRAS induction (**Figure 1F, G**). However, the results showed that the ECAR was increased in doxycycline-treated cells, indicating that lactate production and therefore glycolytic activity is enhanced (**Figure 1H, I**). Furthermore, to investigate the effect of HRAS^{G12V} expression on acetyl-CoA levels, the acetyl-CoA levels were measured. Administration of doxycycline preserved the acetyl-CoA levels, compared to the non-treated cells (**Figure 1E**). Together, these data indicate that doxycycline administration

increases the levels of phosphorylation of downstream HRAS proteins, induces a shift in metabolic flux, and alters the transcriptome in RPE cells. Consequently, this is a relevant model to study nuclear metabolism upon mutant HRAS expression.

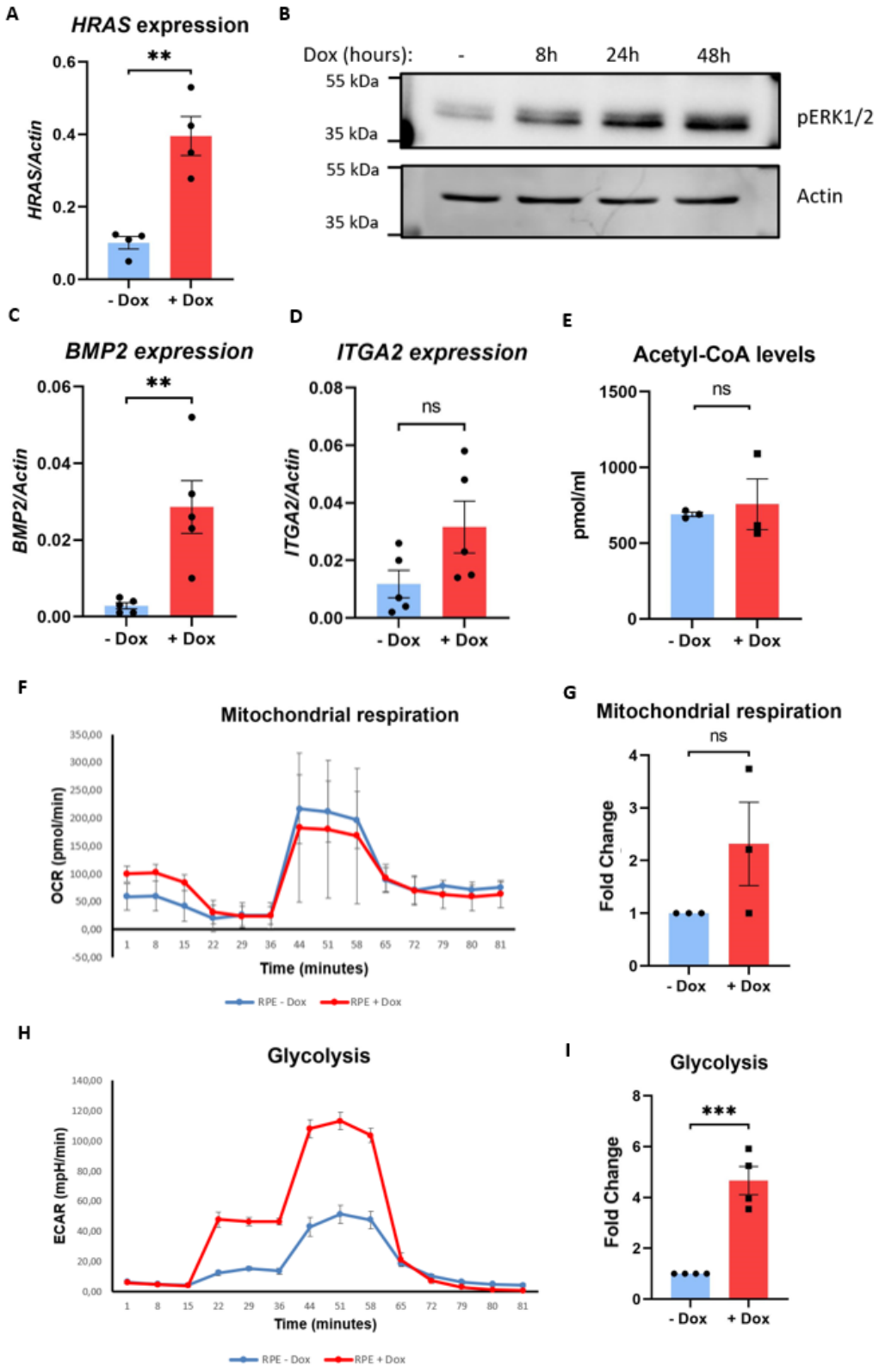

Figure 1. Induction of HRAS^{G12V} in RPE cells results in changes in the transcriptome and metabolism. A) RT-qPCR analysis of HRAS expression in RPE cells after 48h of doxycycline administration. **B**) Western blot analysis of phosphorylated ERK (pERK1/2) and actin in RPE cells treated with 0, 8, 24, or 48 hours of doxycycline. **C**) The expression of *BMP2* was measured by RT-qPCR in RPE cells treated with or without 48h of doxycycline. **D**) The expression of *ITGA2* was measured by RT-qPCR in RPE cells treated with or without 48h of doxycycline. **E**) Intracellular acetyl-CoA levels of RPE cells treated with or without 48h of doxycycline. **F**) Seahorse analysis of the OCR rates after 48h of doxycycline administration in RPE cells (n=4). **G**) Quantification of the fold change of OCR rates in RPE cells treated with 48h of doxycycline compared to non-treated cells. **H**) Seahorse analysis of the ECAR rates after 48h of doxycycline administration in RPE cells (n=4). **I**) Quantification of the fold change of ECAR rates in RPE cells treated with 48h of doxycycline compared to non-treated cells. Data are shown as mean ± SEM. Unpaired Student's t-test was used to analyze statistical significance. Ns means not significant, **P*<0.05, and ***P*<0.01.

Nuclear levels of PDC-E1 are increased upon mutant HRAS expression

Previous research has described the translocation of PDH and ACLY to the nucleus for the generation of acetyl-CoA, important for the acetylation of histones (Wellen et al., 2009; Sutendra et al., 2014). Under hypoxic conditions and glucose deprivation, ACSS2 can translocate to the nuclei and contribute to histone acetylation as well (Busulu et al., 2017; Li et al., 2017). We hypothesized that these acetyl-CoA-producing enzymes might be important for acetyl-CoA production in the nucleus and histone acetylation during mutant HRAS expression. To investigate the nuclear translocation of these enzymes, nuclear extracts were obtained from RPE cells treated with or without doxycycline. After 48h, the nuclear fraction, cytoplasmic fraction, and whole cell lysates were obtained. The protein levels were evaluated using western blot analysis. To confirm that the nuclear and cytoplasmic fractions were pure, tubulin and histone 3 were used as controls. Tubulin is only present in the cytoplasmic fractions and whole cell lysates, whereas histone 3 is present in the nuclear fractions and whole-cell lysates (**Figure 2A**). The results demonstrate nuclear translocation of PDC-E1 after administration of doxycycline (**Figure 2B**). There is no increase in the level of PDC-E1 in the whole-cell lysates of doxycycline-treated and non-treated cells (**Figure 2E**). Although ACLY is increased in the whole cell lysates of doxycycline-treated cells, this increase is not significant on nuclear level (**Figure 2C, F**). The whole cell and nuclear levels of ACSS2 are not changed upon doxycycline administration (**Figure 2D, G**). Thus, these results suggest that PDC-E1 is translocated to the nucleus upon mutant HRAS expression. However, ACLY and ACSS2 do not undergo nuclear translocation after mutant HRAS induction.

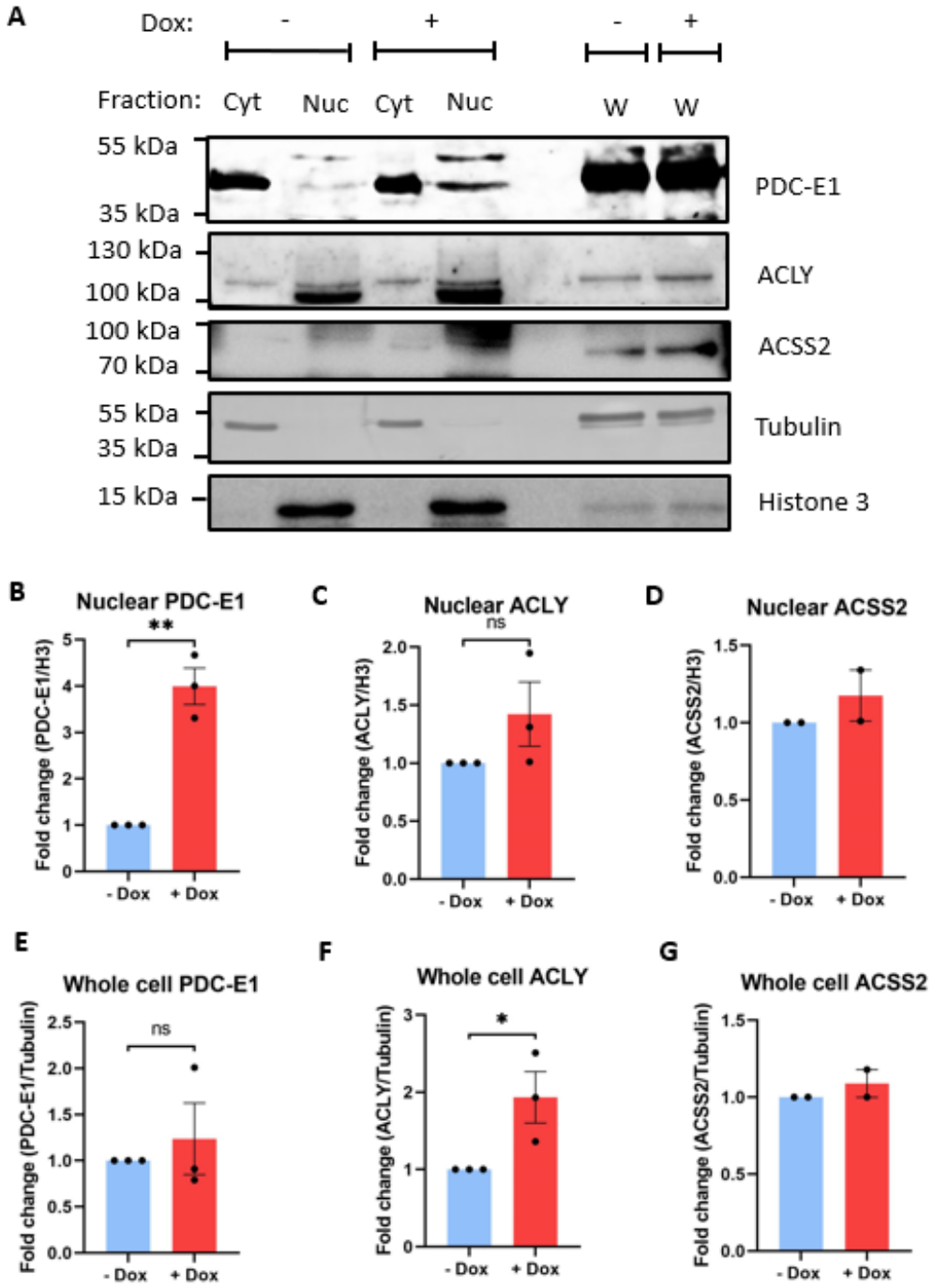

Figure 2. **Nuclear levels of PDC-E1 are increased upon mutant HRAS expression.** RPE cells were plated with or without doxycycline for 48h before the nuclei were isolated. **A**) Western blot analysis of ACLY, ACSS2, PDC-E1, tubulin, and histone 3 levels in cytoplasmic fractions (Cyt), nuclear fractions (Nuc), and whole cell lysates (W). **B-G**) Protein level quantification of PDC-E1, ACLY, and ACSS2, in whole-cell lysates and nuclear fractions of doxycycline-treated cells relative to non-treated cells, normalized by Tubulin or Histone 3 (H3), respectively. Data are shown as mean ± SEM. Unpaired Student's t-test was used to analyze statistical significance. Ns means not significant, **P*<0.05, and ***P*<0.01.

Mutant HRAS expression does not affect the regulation of PDH in RPE cells

Expression of mutant HRAS induces a metabolic switch in RPE cells, significantly increasing glycolysis (**Figure 1I**). Glycolysis generates pyruvate, which is converted to acetyl-CoA by PDH to enter the TCA cycle. The function of mitochondrial PDH is regulated by pyruvate dehydrogenase kinases (PDK). PDK can inhibit PDH activity by phosphorylating the serine-293 residue of the alpha subunit of PDH (Bahal et al., 1993). We evaluated how the expression of mutant HRAS expression affects the regulation of PDH in RPE cells. Western blot analysis was performed on RPE cells induced with 8, 24, and 48 hours of doxycycline to study the levels of PDH and phosphorylated PDH (pPDH). The results showed that the induction of mutant HRAS did not significantly change the total levels of pPDH and PDC-E1 (**Figure 3A-C**). To gain insight in the regulation of PDH in RPE cells, Dichloroacetate (DCA), an inhibitor of PDK, was utilized. The results showed that PDK inhibition significantly decreased pPDH levels after 8, 24, and 48 hours of DCA administration (**Figure 3D, E**). PDC-E1 levels were not significantly changed upon PDK inhibition in RPE cells (**Figure 3F**). Research has shown that PDK is only active in the mitochondria, and not present in the nucleus (Sutendra et al., 2014). In line with this, western blot analysis showed that there is no phosphorylated PDH (pPDH) present in the nuclear fractions of doxycycline-treated and non-treated cells (**Figure 3G**).

Given that PDH is translocated to the nucleus upon mutant HRAS induction, it was hypothesized that the local production of acetyl-CoA by PDH is important for the expression of genes associated with mutant HRAS expression. To evaluate if nuclear PDH is critical for the gene expression of actively transcribed genes *BMP2* and *ITGA2*, an inhibitor of PDH activity, 6,8-bis(benzylthio)octanoic acid (PDHi), was utilized. The results showed that inhibition of PDH using PDHi did not significantly change the expression of *BMP2* and *ITGA2* in mutant HRAS-induced cells (**Figure 3H, I**). In summary, these data show that expression of mutant HRAS does not significantly affect the regulation of PDH in RPE cells. In contrast, inhibition of PDK inhibition significantly decreased the phosphorylation of PDH. The nuclear fractions did not contain pPDH, indicating the mitochondrial activity of PDK. Despite nuclear translocation of PDC-E1, inhibition of PDH did not affect the expression of actively transcribed genes *BMP2* and *ITGA2*.

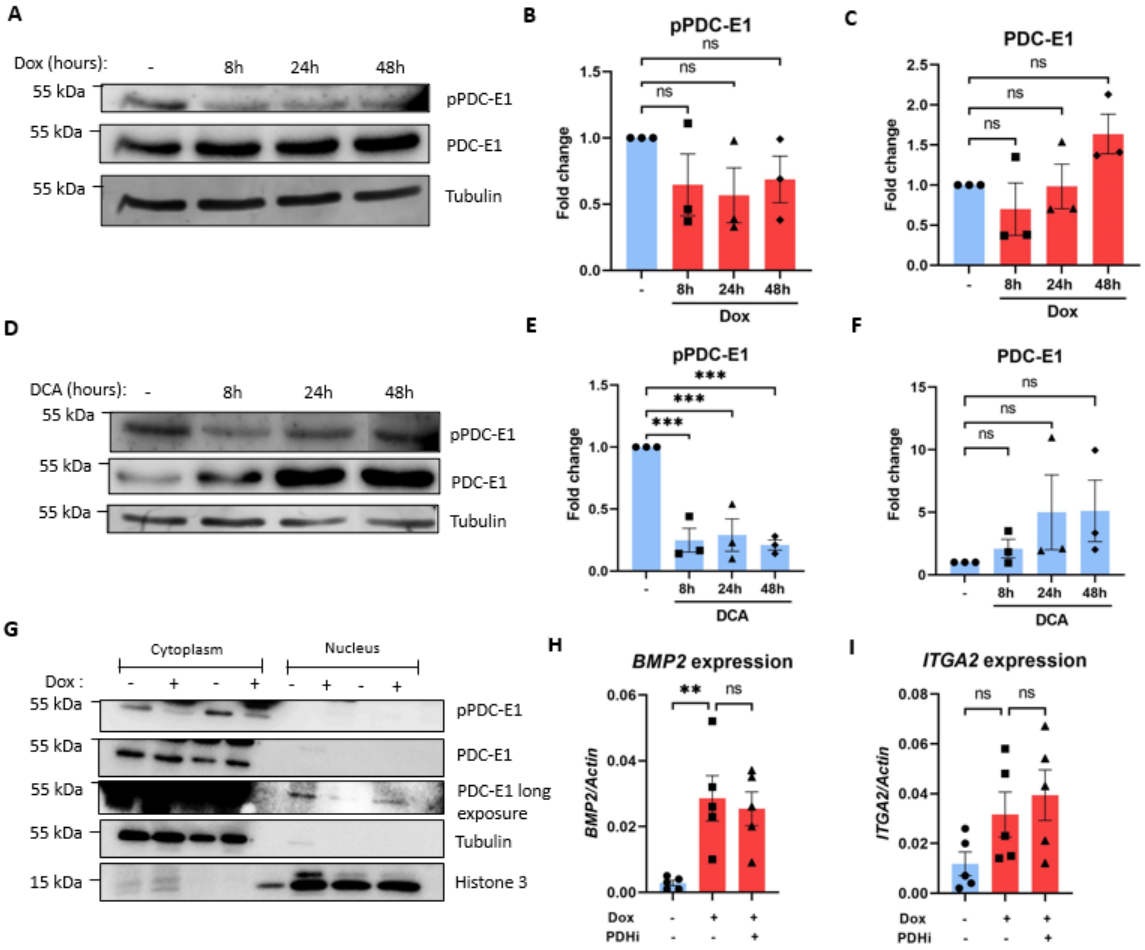

Figure 3. Mutant HRAS expression does not affect the regulation of PDH in RPE cells. A) Western blot analysis of phosphorylated PDC-E1 (pPDC-E1), PDC-E1, and Tubulin after 8, 24, or 48 hours of mutant HRAS induction. **B**) Quantification of pPDC-E1 levels in doxycycline-treated cells compared to non-treated cells. **C**) Quantification of pPDC-E1 levels in doxycycline-treated cells compared to non-treated cells. **D**) Western blot analysis of pPDC-E1, PDC-E1, and Tubulin of RPE cells treated with 8, 24, or 48 hours of DCA (5 µM). **E**) Quantification of pPDC-E1 levels in DCA-treated cells compared to non-treated cells. **F**) Quantification of PDC-E1 levels in DCA-treated cells compared to non-treated cells. **G**) Western blot analysis of pPDC-E1, PDC-E1, tubulin, and histone 3 in cytoplasmic and nuclear fractions of RPE cells with or without 48h of doxycycline administration (n=2). **H, I**) Gene expression of *BMP2* and *ITGA2,* respectively, after 24h of 6,8-bis(benzylthio)octanoic acid (PDHi) administration (150 µM) were measured using qRT-PCR in RPE cells treated with 48h of doxycycline. Data are shown as mean ± SEM. One-way ANOVA with Tukey's multiple comparison test was used to analyze statistical significance, ***P<0.001.

Mutant HRAS expression reconfigures the nuclear interactome of PDH

Since there is nuclear translocation of PDH upon mutant HRAS induction, the interactome of PDH in the nucleus was investigated to gain insight into the role of nuclear PDH (**Figure 2B**)**.** To study the nuclear interactome of PDH, a BioID tool was utilized (**Figure 4A**). This tool consists of a turbo BioID fused to PDC-E1. Upon the addition of biotin, the PDH-BioID, and surrounding proteins are biotinylated. The nuclei of the cells were isolated, and with streptavidin beads, these biotinylated proteins were pulled down. Western blot analysis showed that the PDH-BioID is present in the cytoplasmic and nuclear fractions of RPE cells and can biotinylate (**Figure 4B**). As a negative control to reduce noise, a second BioID tool was utilized consisting of a BioID fused to LaminB, which is a protein located also in the nucleus on the heterochromatin (**Figure 4A**). The BioID contains an HA-tag, only present in the LaminB-BioID. The results showed that the LaminB-BioID is present in the nucleus of RPE cells and can biotinylate (**Figure 4C**).

RPE cells containing the PDH-BioID or the LaminB-BioID were treated with or without doxycycline. After 48h the cells were harvested, and nuclear isolation was performed. The samples were sent for LC-MS-based proteomics. The number of proteins identified in the LaminB-BioID samples were lower than in the PDH-BioID samples (**Figure 4D**). Principal component analysis (PCA) of these data demonstrates that the LaminB-BioID samples and PDH-BioID samples cluster separately (**Figure 4E**). This indicates that there distinct differences between the nuclear interactome of LaminB and PDH. RPE cells containing the PDH-BioID have significantly enriched PDC-E1 in the nuclear interactome.

To evaluate specific changes in the nuclear interactome of PDH upon mutant HRAS induction, we compared the proteins significantly enriched in the nuclear interactome of PDH relative to LaminB in both doxycycline-treated and non-treated cells. The Venn-Diagram analysis revealed that there are 146 genes commonly enriched in the nuclear interactome of PDH in doxycycline-treated and non-treated cells, indicating that their proteins are not affected by mutant HRAS expression (**Figure 4H**). There are 144 proteins present only in the interactome of PDH in the non-treated cells. 104 proteins are only present in the interactome of PDH in doxycycline-treated cells, suggesting that these genes are influenced by the expression of mutant HRAS (**Figure 4H**). This suggests that the changes observed upon mutant HRAS expression in the PDH interactome are specific for PDH and not due to nonspecific protein interactions. In accordance with previous research that showed the association between PDH and histone acetyltransferase p300, we found p300 (EP300) to be significantly enriched in the interactome nuclear of PDH (Mocholi et al., 2023) (**Figure 4F**). Interestingly, proteomics data revealed that PKM, a glycolytic enzyme, is present in the nuclear interactome of

PDH (**Figure 4G**). This is in line with other studies that found that PDH forms a complex with PKM2 that can facilitate pyruvate production for PDH to convert to acetyl-CoA (Matsunda et al., 2015).

Proteomics analysis identified how mutant HRAS expression affects proteins that interact with nuclear PDH. The findings showed how different proteins are in close proximity to nuclear PDH in doxycycline-treated and non-treated cells (**Figure 4I, J**). In doxycycline-treated cells, gene ontology (GO)-term analysis of molecular function revealed that the enriched proteins close to PDH are related to transcription factor binding and activity (**Figure 4K**). The proteins close to nuclear PDH in non-treated cells were associated with different functional roles. GO-term analysis of molecular function showed that proteins in close proximity to nuclear PDH in non-treated cells play a role in protein serine kinase activity, histone modifying activity and DNA-binding transcription factor binding (**Figure 4L**). Furthermore, GO-term analysis of biological processes on genes enriched near nuclear PDH in doxycycline-treated cells showed that there is enrichment of proteins involved in cell cycle, transcription, and chromosome localization (**Figure 4M**). Similarly, GO-term analysis of biological processes on genes enriched near nuclear PDH in non-treated cells revealed that there is enrichment of proteins involved in cell cycle processes (**Figure 4N**). This suggests that PDH is associated with proteins involved in cell cycle regulation, regardless of mutant HRAS expression. Together, these data show that, for the first time, we can identify the interactome of a metabolic enzyme in the nucleus. These findings reveal that mutant HRAS expression reconfigured the nuclear interactome of PDH, increasing enrichment of proteins involved in cell cycle regulation and transcription factor regulation.

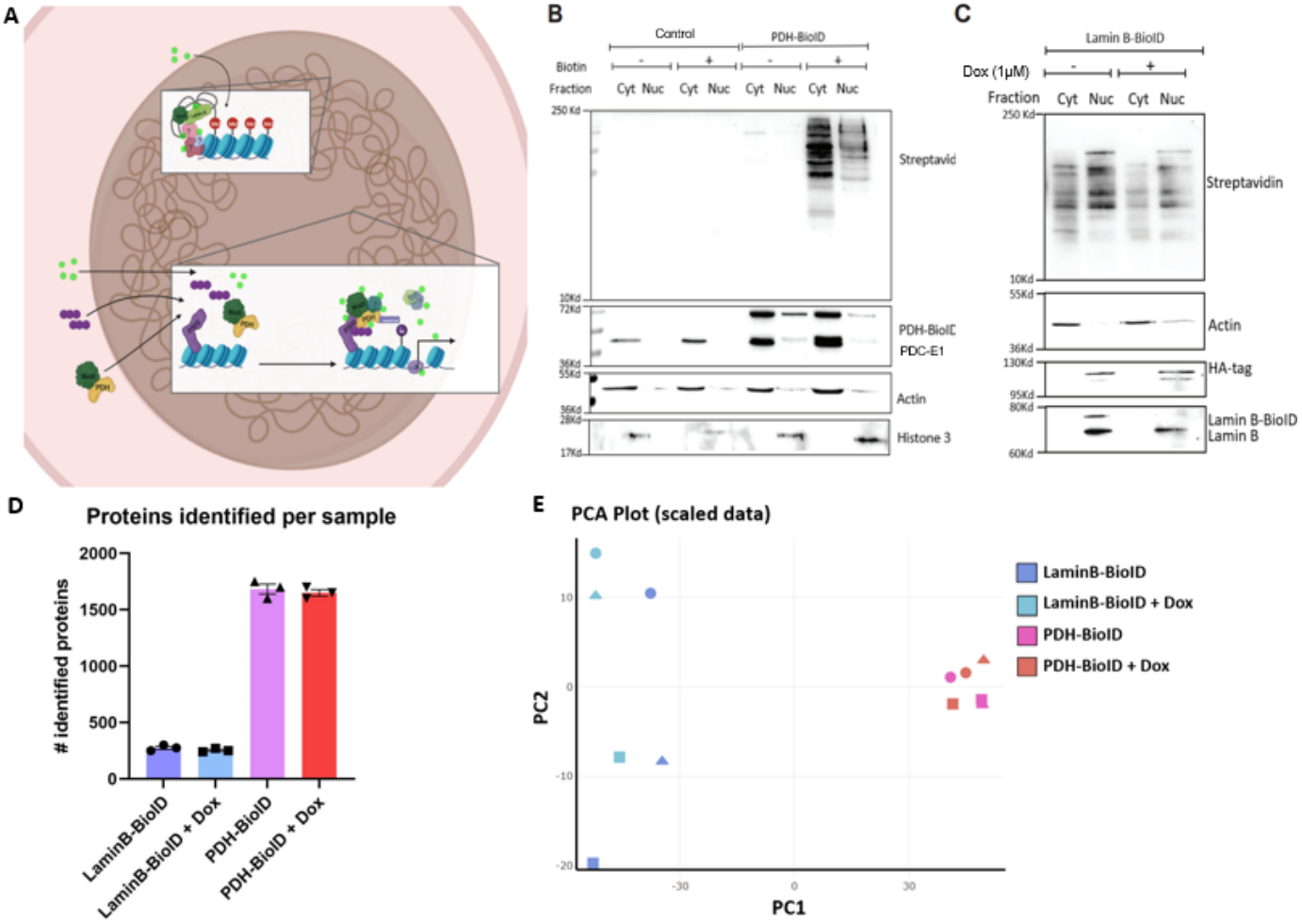
A
B
Control
PDH-BioID
Biotin
Fraction
Cyt Nuc Cyt Nuc Cyt Nuc Cyt Nuc
250 Kd
Streptavid
PDH-BioID
PDC-E1
Actin
Histone 3
C
Lamin B-BioID
Dox (1µM)
Fraction
Cyt Nuc Cyt Nuc
Streptavidin
Actin
HA-tag
Lamin B-BioID
Lamin B
D
Proteins identified per sample
identified proteins
LaminB-BioID
LaminB-BioID + Dox
PDH-BioID
PDH-BioID + Dox
E
PCA Plot (scaled data)
PC1
PC2
LaminB-BioID
LaminB-BioID + Dox
PDH-BioID
PDH-BioID + Dox
F
Differential enrichment of proteins in the interactome of PDH-BioID vs LaminB-BioID
Intensity: iBAQ. Imputation: Gaussian (shift = 1.8 and scale = 0.3)
P-value (-log10)
Fold Change (log2)
PDH-BioID
LaminB-BioID
G
Differential enrichment of proteins in the interactome of PDH-BioID + Dox vs LaminB-BioID + Dox
Intensity: iBAQ. Imputation: Gaussian (shift = 1.8 and scale = 0.3)
P-value (-log10)
Fold Change (log2)
PDH-BioID +Dox
LaminB-BioID +Dox
H
Significantly enriched genes in the nuclear interactome
144
146
104
PDH-BioID
PDH-BioID + Dox

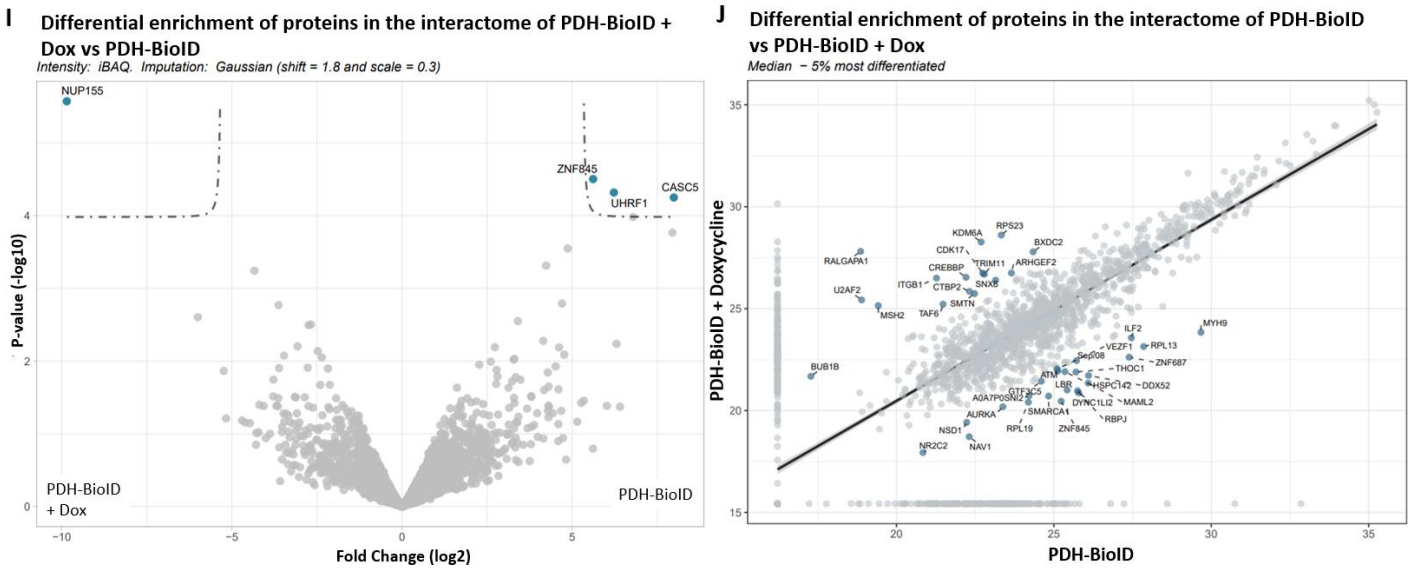

K

Gene-ontology analysis of molecular function on genes enriched close to nuclear PDH in doxycycline-treated cells.

	Gene ontology	
-log (P-value)	0 5 10	
Transcription coregulator activity		p=E-8
Transcription factor binding		p=E-8
Transcription coactivator binding		p=E-7
Chromatin binding		p=E-5

L

Gene-ontology analysis of molecular function on genes enriched close to nuclear PDH in non-treated cells.

	Gene ontology	
-log (P-value)	0 5 10	
Protein serine kinase activity		p=E-5
Histone modifying activity		p=E-5
DNA-binding transcription factor binding		p=E-5
GTPase binding		p=E-4

M

Gene-ontology analysis of biological processes on genes enriched close to nuclear PDH in doxycycline-treated cells.

	Gene ontology	
-log (P-value)	0 5 10	
Positive regulation of DNA-templated transcription		p=E-10
Positive regulation of RNA biosynthetic process		p=E-10
Cell cycle process		p=E-9
Protein-DNA complex organization		p=E-9

N

Gene-ontology analysis of biological processes on genes enriched close to nuclear PDH in non-treated cells.

	Gene ontology	
-log (P-value)	0 5 10	
Mitotic cell cycle		p=E-13
Cell cycle process		p=E-13
Regulation of cell cycle		p=E-10
DNA metabolic process		p=E-9

Figure 4. Mutant HRAS expression induces reconfiguration of the nuclear interactome of PDH. RPE cells containing the PDH-BioID or LaminB-BioID were treated with or without doxycycline. After 48h the nuclei were isolated, the BioID complexes were pulled down and sent for LC-MS-based proteomics. **A**) Schematic representation of the BioID constructs of the PDH-BioID and the LaminB-BioID. **B**) Western blot analysis of streptavidin, PDH-BioID, PDC-E1, actin, and histone 3 in RPE cells, and RPE cells containing the PDH-BioID treated with or without D-biotin (50 µM). **C**) Western blot analysis of streptavidin, actin, HA-tag, LaminB, and LaminB-BioID in RPE cells containing the LaminB-BioID treated with or without doxycycline. **D**) The number of identified proteins in the LC-MS-based proteomics samples. **E**) Principal component analysis (PCA) of the data. **F**) Volcano plot showing differential protein enrichment near PDH vs LaminB in non-treated cells. **G**) Volcano plot showing differential protein enrichment near PDH vs LaminB in doxycycline-treated cells. **H**) Venn diagram

analysis of all proteins enriched near the PDH-BioID relative to the LaminB-BioID in doxycycline-treated cells compared to non-treated cells. **I**) Volcano plot showing differential protein enrichment near PDH in doxycycline-treated cells vs non-treated cells. **J**) Scatter plot showing differential protein enrichment of proteins in the interactome of PDH in doxycycline-treated vs non-treated cells. **K**) Gene Ontology analysis on molecular function, enriched in the nuclear interactome of PDH in doxycycline-treated cells relative to non-treated cells, ranked by P-value. **L**) Gene Ontology analysis on molecular function, enriched in the nuclear interactome of PDH in non-treated cells relative to doxycycline-treated cells, ranked by P-value. **M**) Gene Ontology analysis on biological process, enriched in the nuclear interactome of PDH in doxycycline-treated cells relative to non-treated cells, ranked by P-value. **N**) Gene Ontology analysis on biological process, enriched in the nuclear interactome of PDH in non-treated cells relative to doxycycline-treated cells, ranked by P-value. Data are shown as mean ± SEM (n=3).

Nuclear PDC-E1 is located near promotor regions of actively transcribed genes upon mutant HRAS expression

The data suggests that PDH is translocated to the nucleus upon mutant HRAS induction, which reconfigures the nuclear interactome of PDH (**Figure 4J**). To investigate the location of PDH on the chromatin and the associated genes, ChIP-qPCR was performed. It is hypothesized that PDH plays a role in the active transcription of relevant genes regulated by the expression of $HRAS^{G12V}$. Again, the BioID tool was utilized to allow the labeling of proteins close to PDH (**Figure 4A**). Since it is hypothesized that PDH is located close to the DNA, it makes biotinylation of proteins on the DNA possible. The biotinylated proteins were crosslinked to the DNA, and using streptavidin beads these biotinylated complexes can be pulled down and analyzed. Previous research has performed RNA-sequencing, showing that $HRAS^{G12V}$ expression in RPE cells changes the transcriptome (Segeren et al., 2022). *BMP2* and *ITGA2* are upregulated upon mutant HRAS expression in RPE cells (**Figure 1C, D**). ChIP-qPCR results show that mutant HRAS-induced cells have enriched PDH near the promotor regions of actively transcribed genes *BMP2* and *ITGA2* (**Figure 5A, B**). The RPE cells containing the LaminB-BioID did not show enrichment of LaminB near promotor genes sites of *BMP2* and *ITGA2* (**Figure 5A, B**). Subsequently, the samples were sent for ChIP-sequencing to investigate the associated chromatin location of PDH. However, these results are not included in the report, because analysis has not yet been conducted. In conclusion, these data demonstrate that PDH is located close to the promotor regions of actively transcribed genes, *BMP2* and *ITGA2*, regulated by mutant HRAS expression (**Figure 5C**).

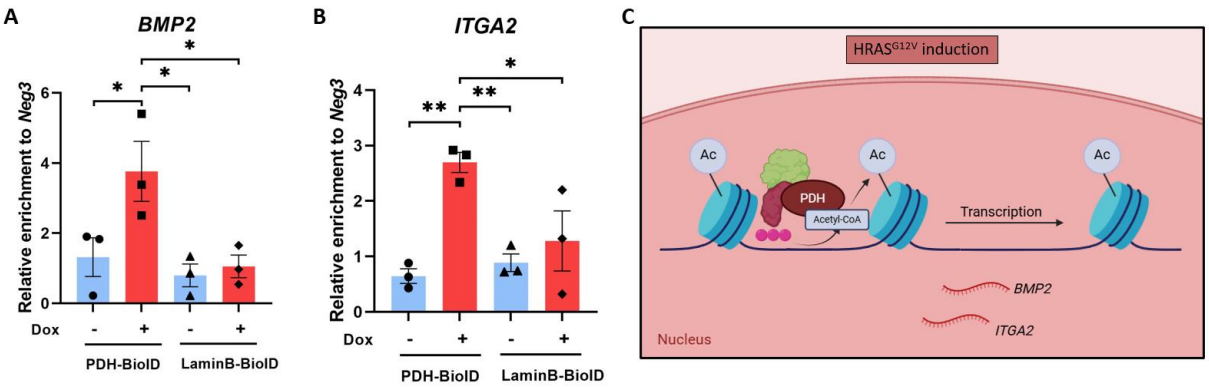

Figure 5. Nuclear PDC-E1 is located near promotor regions of actively transcribed genes *BMP2* and *ITGA2* upon mutant HRAS expression. A) The relative enrichment of PDH and LaminB near *BMP2* promotor regions upon mutant HRAS-induction was analyzed by ChIP-qPCR. The enrichment was normalized to a negative region (*Neg3*). **B**) The relative enrichment of PDH and LaminB near *ITGA2* promotor regions upon mutant HRAS-induction was analyzed by ChIP-qPCR. The enrichment was normalized to a negative region (*Neg3*). **C**) Schematic overview of PDH located near promotor regions of *BMP2* and *ITGA2* upon mutant HRAS induction. Data are shown as mean ± SEM. One-way ANOVA with Tukey's multiple comparison test was used to analyze statistical significance, **P*<0.05, and ***P*<0.01.

DISCUSSION

The activation of oncogenes induces changes in the remodeling of the epigenome and the transcriptome, causing for cancer cells to uncontrollably proliferate and metastasize (Hanahan & Weinberg, 2011). Changes in the epigenome can be facilitated by acetyl-CoA, utilized for histone acetylation. Previous studies have suggested a role for enzymes that produce acetyl-CoA in facilitating gene transcription (Wellen et al., 2008; Sutendra et al., 2014; Mocholi et al., 2023). The role of acetyl-CoA-producing enzymes during mutant HRAS expression is not very well known. This report shows that upon mutant HRAS induction, acetyl-CoA-producing enzyme PDH is translocated to the nucleus (**Figure 2B**). The total levels of acetyl-CoA are not changed upon mutant HRAS expression (**Figure 1E**). However, this does not preclude local changes of acetyl-CoA levels in the nucleus. In the nucleus, proteomics analysis revealed that the interactome of PDH is reconfigured by mutant HRAS induction (**Figure 4I**). The reconfiguration shows an enrichment of transcription factor binders and activators present in the interactome of PDH in mutant HRAS-induced cells (**Figure 4J**). Furthermore, the results show that PDH is enriched near the promotor regions actively transcribed genes regulated by the expression of $HRAS^{G12V}$ (**Figure 5A, B**). These findings highlight the role of nuclear PDH during mutant HRAS induction and suggest that PDH might be a potential therapeutic target to interfere with to try to inhibit oncogenic transformation.

To study the role of acetyl-CoA-producing enzymes during mutant HRAS induction, RPE cells with inducible $HRAS^{G12V}$ were utilized. In accordance with previous research, the administration of doxycycline to RPE cells increased the expression of HRAS and phosphorylation of downstream proteins (Segeren et al., 2022) (**Figure 1A, B**). Cancer cells often have increased aerobic glycolysis, called the Warburg effect (Warburg et al., 1927). Although mitochondrial respiration is not significantly changed upon mutant HRAS expression, glycolysis was significantly increased after $HRAS^{G12V}$ induction (**Figure 1I, J**). This is in line with earlier research (Myallymäki et al., 2024). Interestingly, acetyl-CoA levels were not changed after mutant HRAS induction (**Figure 1K**). This indicates that mutant HRAS expression does not increase the production of acetyl-CoA. However, it could be possible that there is local production of acetyl-CoA in the nucleus. Measuring acetyl-CoA levels specifically in the nucleus could give insight in how mutant HRAS changes acetyl-CoA production.

Previous research has shown that several acetyl-CoA-producing enzymes are present in the nucleus and able to produce acetyl-CoA to facilitate histone acetylation (Sutendra et al., 2014; Wellen et al., 2009). The results indicate that PDH is translocated to the nucleus in $HRAS^{G12V}$-induced RPE cells (**Figure 2B**). There was no significant increase in nuclear ACLY or ACSS2 after mutant HRAS induction (**Figure 2C, D**). This might suggest that the translocation of PDH to the nucleus could have a role in the epigenome remodeling induced by mutant HRAS expression. The mechanism of how PDH is translocated remains unknown. Earlier research proposed a role for HSP70 in the transportation of PDH (Sutendra et al., 2014; Mocholi et al., 2023). Recently, a study revealed how mitochondria can locate around the nucleus, allowing transportation of PDH (Zervopoulos et al., 2022). Our proteomics data analysis revealed that PDH is associated with nuclear pore complex NUP155 in the nucleus (**Figure 4F**). NUP155 can transport proteins in the nucleus and has been associated with regulating cancer-pathways (Holzer et al., 2019). This pore nuclear complex could possibly have a role in the nuclear transportation of PDH. However, further research should be conducted to investigate this mechanism.

Furthermore, the impact of mutant HRAS expression on the regulation of PDH in RPE cells was studied. PDH activity is mainly regulated through phosphorylation by PDK (Bahal et al., 1993). The results show that $HRAS^{G12V}$ expression did not significantly change the levels of PDH and pPDH (**Figure 3B, C**). This might suggest that mutant HRAS expression does not alter PDH regulation in RPE cells. Inhibition of PDK decreased the total levels of pPDH after only 8h (**Figure 3E**). The findings demonstrate that pPDH is not present in the nuclei (**Figure 3G**). In line with earlier research, this might suggest that mitochondrial PDH is regulated differently from nuclear PDH (Sutendra et al., 2014). Since PDH might play a role in the epigenome remodeling induced by mutant HRAS

expression, it was hypothesized that targeting PDH might interfere with the expression of actively transcribed genes *BMP2* and *ITGA2*. 6,8-bis(benzylthio)octanoic acid is an analog for the lipoate coenzyme that is important for function of PDH, and was shown to interfere with mitochondrial metabolism, inducing cell death in tumor cells (Zachar et al., 2011). 6,8-bis(benzylthio)octanoic acid administration in doxycycline-treated cells did not change the expression of *BMP2* and *ITGA2* (**Figure 3H, I**). However, it is not known if this inhibitor also affects PDH function in the nucleus. Therefore, it is difficult to draw conclusions on the effect of PDH on the expression of genes from these results.

To investigate the interactome of nuclear PDH, LC-MS-based proteomics analysis was performed. The number of identified proteins in the LaminB-BioID interactomes were lower than the number in the PDH-BioID interactomes (**Figure 4D**). However, LaminB is located in a region devoid of active transcription. Therefore, it is expected that the number of proteins near LaminB lower than near PDH. Proteomics analysis of the interactome of nuclear PDH revealed that induction of mutant HRAS reconfigured the interactome of PDH (**Figure 4J**). The nuclear interactome of PDH contains proteins involved in cell cycle regulation in mutant HRAS induced and non-induced cells. This is in line with earlier research that showed that PDH regulates cell cycle progression by enhancing S-phase entry (Sutendra et al., 2014). Since there is enrichment of proteins close to PDH involved in transcription factor and cell-cycle regulation, it might indicate that nuclear PDH could play a role in transcriptional reprogramming upon mutant HRAS activation (**Figure 4K**).

Although the nuclear presence of PDC-E2 and PDC-E3 has been reported in several studies, the proteomics data did not show the presence of these enzymes in the interactome of the PDH-BioID (Sutendra et al., 2014; Russo et al., 2024). However, the fact that we did not identify the other members of the PDH complex does not preclude their presence. Additionally, the BioID tool was used to study the associated chromatin location of PDH. ChIP-qPCR results revealed that PDH is enriched near the promotor genes of actively transcribed genes *BMP2* and *ITGA2* upon mutant HRAS induction. This enrichment was not shown with the LaminB-BioID, indicating that the relocation is specific for PDH (**Figure 5A, B**). These data show that the location of nuclear PDH changes upon mutant HRAS-expression. Sequencing analysis of the ChIP-DNA will give insight in genes associated with nuclear PDH.

To conclude, this report highlights the role of nuclear PDH during mutant HRAS expression. While the results only show significant nuclear translocation of PDH after in $HRAS^{G12V}$-induced RPE cells, further research could investigate the potential interplay between acetyl-CoA-producing enzymes that might facilitate gene transcription. The induction of mutant HRAS has also been reported to induce senescence, a process known to induce epigenome remodeling (Serrano et al., 1997; Nacarelli et al.,

2017). Therefore, it can be relevant to study the role of nuclear PDH in transcriptional regulation in senescence. Understanding the mechanisms of metabolic enzyme PDH in the context of nuclear metabolism in mutant HRAS transformation is of importance to explore new avenues for targeted treatment of cancer.

REFERENCES

Abramoff, M.D., Magalhaes, P.J. & Ram, S.J. (2004). Image processing with ImageJ. *Biophotonics International, 11*, 36-42.

Alberts, B., Bray, D., Hopkin, K., Johnson, A.D., Lewis, J., Raff, M., et al. (2018). *Essential biology of the cell*. 5th edition. Twitchell, B. & Morales, M. W. W. Norton & Company. 560.

Bahal, R.H., Buxton D.B., Robertson, J.G. & Olson, M.S. (1993). Regulation of the pyruvate dehydrogenase multienzyme complex. *Annual review of nutrition, 13,* 497-520.

Bar-Peled, L. & Kory, N. (2022). Principles and functions of metabolic compartmentalization. *Nature metabolism, 4,* 1232-1244.

Bulusu, V., Tumanov, S., Michalopoulou, E., van den Broek, N.J., Dhayade, S.D., Schug, Z.T., et al. (2017). Acetate recapturing by nuclear acetyl-CoA synthetase 2 prevents loss of histone acetylation during oxygen and serum limitation. *Cell reports, 18,* 647-648.

Campbell, S.L. & Wellen, K. E. (2018). Metabolic signaling to the nucleus in cancer. *Molecular Cell, 71,* 398-408.

Davis, H., Raja, E., Miyazonom K., Tsubakihara, Y. & Moustakas, A. (2015). Mechanisms of action of bone morphogenetic proteins in cancer. *Cytokine Growth Factor Reviews, 27*, 81-92.

Der, C.J., Krontiris, T.G. & Cooper, G.M. (1982). Transforming genes of human bladder and lung carcinoma cell lines are homologous to the ras genes of Harvey and Kirsten sarcoma viruses. *Proceedings of the National Academy of Sciences, 79*, 3637-3640.

Falkenberg, K.J. & Johnstone, R.W. (2014). Histone deacetylases and their inhibitors in cancer, neurological diseases and immune disorders. *Nature Reviews Drug Discovery, 13*, 673-691.

Gregori, A., Bergonzi, C., Capula, M., Mantini, G., Khojasteh-Leylakoohi, F., Comandatore, A., et al. (2023). Prognostic significance of integrin subunit alpha 2 (ITGA2) and role of mechanical cues in resistance to gemcitabine in pancreatic ductal adenocarcinoma (PDAC). *Cancers, 15*, 628.

Hanahan, D. & Weinberg, R.A. (2011). Hallmarks of cancer: the next generation. *Cell, 144,* 646-674.

Holzer, K., Ori, A., Cooke, A., Dauch, D., Drucker, E., Riemenschneider, P., et al. (2019). Nucleoporin Nup155 is part of the p53 network in liver cancer. *Nature Communications, 10,* 2147.

Hosios, A.M., Hecht, V.C., Danai, L.V., Johnson, M.O., Rathmell, J.C., Steinhauser, M.L., et al. (2016). Amino acids rather than glucose amount for the majority of cell mass in proliferating mammalian cells. *Developmental Cell, 36,* 540-549.

Kroemer, G. & Pouyssegur, J. (2008). Tumor cell metabolism: cancer's Achilles heel. *Cancer Cell, 13,* 472-482.

Lee, D.Y., Hayes, J.J., Pruss, D. & Wolffe, A.P. (1993). A positive role for histone acetylation in transcription factor access to nucleosomal DNA. *Cell, 72,* 73-84.

Li, W., Long, Q., Wu, H., Zhou, Y., Duan, L., Yuan, L., et al. (2022). Nuclear localization of mitochondrial TCA cycle enzymes modulates pluripotency via histone acetylation. *Nature Communications, 13,* 7414.

Li, X., Yu, W., Qian, X., Xia, Y., Zheng, Y., Lee, J.H., et al. (2017). Nucleus-translocated ACSS2 promotes gene transcription for lysosomal biogenesis and autophagy. *Molecular Cell, 66*, 684-697.

Liu, X.S., Little, J.B. & Yuan, Z.M. (2015). Glycolytic metabolism influences global chromatin structure. *Oncotarget, 6*, 4214-4225.

Matsunda, S., Adachi, J., Ihara, M., Tanuma, N., Shima, H., Kakizuka, A., et al. (2015). Nuclear pyruvate kinase M2 complex serves as a transcriptional coactivator of arylhydrocarbon receptor. *Nucleic Acid Research, 44,* 636-647.

Milne, J.L.S. (2013). *Encyclopaedia of Biological Chemistry*. 2nd Edition. Lennarz, W.J. & Lane, D.M. Academic Press, 321-328.

Mocholi, E., Russo, L., Gopal, K., Ramstead, A.G., Hochrein, S.M., Vos, H.R., et al. (2023). Pyruvate metabolism controls chromatin remodeling during $CD4^+$ T cell activation. *Cell reports, 42*, 112583.

Moussaieff, A., Rouleau, M., Kitsberg, D., Cohen, M., Levy, G., Barasch, D., et al. (2015). Glycolysis-mediated changes in acetyl-CoA and histone acetylation control the early differentiation of embryonic stem cells. *Cell Metabolism, 21*, 392-402.

Myllymäki, H., Kelly, L., Elliot, A.M., Carter, R.N., Johansson, J.A., Chang, K.Y., et al. (2024). Preneoplastic cells switch to Warburg metabolism from their inception exposing multiple vulnerabilities for targeted elimination. *Oncogenesis, 12*, 7.

Nacarelli, T., Liu, P. & Zhang, R. (2017). Epigenetic basis of cellular senescence and its implications on aging. *Genes, 8*, 343.

Parada, L.F., Tabin, C.J., Shih, C. & Weinberg, R.A. (1982). Human EJ bladder carcinoma oncogene is homologue of Harvey sarcoma virus ras gene. *Nature, 297*, 474-478.

Prior, I.A., Lewis, P.D. & Mattos, C. (2012). A comprehensive survey of Ras mutations in cancer. *Cancer research, 72*, 2457-2467.

Pylayeva-Gupta, Y., Grabocka, E. & Bar-Sagi, D. (2011). RAS oncogenes: weaving a tumorigenic web. *Nature reviews cancer, 11,* 761-774.

Ralston, A. & Brown, W. (2008). Chromatin remodeling and DNase 1 sensitivity. *Nature Education, 1,* 15.

Russo, M., Gualdrini, F., Vallelonga, V., Mitro, N., Ghisletti, S., Natoli, G., et al. (2024). Acetyl-CoA production by Mediator-bound 2-ketoacid dehydrogenases boost *de novo* histone acetylation and is regulated by nitric oxide. *Molecular Cell, 84,* 967-980.

Serrano, M., Lin, A.W., McCurrach, M.E., Beach, B. & Lowe, S.W. (1997). Oncogenic ras provokes premature cell senescence associated with accumulation of p53 and $p16^{INK4a}$. *Cell, 88,* 593-602.

Schlug, Z.T., Vande Voorde, J. & Gottlieb, Y. (2016) The metabolic fate of acetate in cancer. *Nature Reviews Cancer, 16,* 708-717.

Shen, H. & Laird, P.W. (2013). Interplay between the cancer genome and epigenome. *Cell, 153*, 38-55.

Sivanand, S., Rhoades, S., Jiang, Q., Lee, J.V., Benci, J., Zhang, J., et al. (2017). Nuclear acetyl-CoA production by ACLY promotes homologous recombination. *Molecular Cell, 67*, 252-265.

Sivanand, S., Viney, I. & Wellen, K.E. (2018). Spatiotemporal control of acetyl-CoA metabolism in chromatin regulation. *Trends in Biochemical Sciences, 43*, 61-74.

Sun, R.C., Dukhande, V.V., Zhou, Z., Young, LE.A., Emanuelle, S., Brainson, C.F., et al. (2019). Nuclear Glycogenolysis modulates histone acetylation in human non-small cell lung cancer. *Cell metabolism, 30,* 903-916.

Sutendra, G., Kinnaird, A., Dromparis, P., Paulin, R., Stenson, T.H., Haromy, A., et al. (2014). A nuclear pyruvate dehydrogenase complex is important for the generation of acetyl-CoA and histone acetylation. *Cell, 158,* 84-97.

Wellen, K.E., Hatzivassiliou, G., Sachdeva, U.M., Bui, T.V., Cross, J.R. & Thompson. (2009). ATP-lyase links cellular metabolism to histone acetylation. *Science, 324,* 1021.

Warburg, O., Wind, F. & Negelein, E. (1927). The metabolism of tumors in the body. *The Journal of General Physiology, 8,* 519-530.

Zachar, Z., Marecek, J., Maturo, C., Gupta, S., Stuart, S.D., Howell, K., et al. (2011). Non-redox-active lipoate derivates disrupt cancer cell mitochondrial metabolism and are potent anticancer agents in vivo. *Journal of Molecular Medicine, 89*, 1137-1148.

Zervopoulos, S.D., Boukouris, A.E., Saleme, B., Haromy, A., Tejay, S., Sutendra, G., et al. (2022). MFN2-driven mitochondria-to-nucleus tethering allows a non-canonical nuclear entry pathway of the mitochondrial pyruvate dehydrogenase complex. *Molecular Cell, 82,* 1066-1077.

Zhou, W., Niu, Y.J., Nie, Z.W., Kim, J.Y., Xu, Y.N., Yan, C.G. et al. (2020). Nuclear accumulation of pyruvate dehydrogenase alpha 1 promotes histone acetylation for zygotic genome activation in porcine embryos. *Biochimica et Biophysica Acta (BBA) - Molecular Cell Research, 1867*, 118648.

SUPPLEMENTARY MATERIAL

Table S1: Western blot antibodies

Antibody	**Company**	**Catalogue number**
ACSS2	Abcam	ab66038
ATP Citrate Lyase	Cell Signaling	4332S
β-Actin	Santa Cruz Biotechnology	sc-47778
HA-tag	Genscript	A00168
Histone H3	Active motif	39064
LaminB2	Cell Signaling	13435s
PDHA1	Proteintech	18068-1-AP
Anti-phosphoPDHE1-A type I (Ser300)	Abcam	Abs194
P44/42 MAP Kinase	Signalway antibody	11246
Streptavidin	Abcam	Ab7403
Tubulin	Sigma	047M4789V

Table S2: ChIP-qPCR primer sequences

Primer	**Sequence**
BMP2 forward primer (5'-3')	GCTCCGCTTCCCACACC
BMP2 reverse primer (5'-3')	GTGATCCACTCGGCGCTG
ITGA2 forward primer (5'-3')	CCCAAACACAGGTCTGTTCC

ITGA2 reverse primer (5’-3’)	AAGGAAGTCAGCCAGGTTTCA
Neg3 forward primer (5’-3’)	GAGCCAGGGTTTCTCTGATTC
Neg3 reverse primer (5’-3’)	CCTCAGTGATCAGCCCTAAATG

Table S3: RT-qPCR primer sequences

Primer	**Sequence**
BMP2 forward primer (5’-3’)	GGAACGGACATTCGGTCCTT
BMP2 reverse primer (5’-3’)	ACCATGGTCGACCTTTAGGAC
ITGA2 forward primer (5’-3’)	CACAAAGACACAGGTGGGT
ITGA2 reverse primer (5’-3’)	TGGGATGTCTGGGATGTTGC
Actin forward primer (5’-3’)	CTGGAACGGTGAAGGTGACA
Actin reverse primer (5’-3’)	AAGGGACTTCCTGTAACAATGCA
HRAS forward primer (5’-3’)	GGAAGCAGGTGGTCATTGAT
HRAS reverse primer (5’-3’)	ATGGCAAACACACACAGGAA